International Journal of Thermophysics, Vol. 24, No. 6, November 2003 (© 2003)

The Viscosity of Seven Gases Measured with a Greenspan Viscometer

J. J. Hurly,[1,2] K. A. Gillis,[1] J. B. Mehl,[3] and M. R. Moldover[1]

Received May 19, 2003

The viscosity of seven gases (Ar, CH_4, C_3H_8, N_2, SF_6, CF_4, C_2F_6) was determined by interpreting frequency-response data from a Greenspan acoustic viscometer with a detailed model developed by Gillis, Mehl, and Moldover. The model contains a parameter ϵ_r that characterizes the viscous dissipation at the ends of the viscometer's duct. It was difficult to determine ϵ_r accurately from dimensional measurements; therefore, ϵ_r was adjusted to fit the viscosity of helium on the 298 K isotherm (0.6 MPa $< p <$ 3.4 MPa). This calibration was tested by additional viscosity measurements using four, well-studied, polyatomic gases (CH_4, C_2H_6, N_2, and SF_6) near 300 K and by measurements using argon in the range 293 K $< T <$ 373 K. For these gases, all of the present results agree with reference values to within $\pm 0.5\%$ ($\pm 0.4\%$ in the limit of zero density). The viscosities of CF_4 and C_2F_6 were measured between 210 and 375 K and up to 3.3 MPa with average uncertainties of 0.42 and 0.55%, respectively. At the highest density studied for CF_4 (2746 mol·m^{-3}), the uncertainty increased to 1.9%; of this 1.9%, 0.63% resulted from the uncertainty of the thermal conductivity of CF_4, which other researchers estimated to be 2% of its value at zero density. As an unexpected bonus, the present Greenspan viscometer yielded values of the speed of sound that agree, within $\pm 0.04\%$, with reference values.

KEY WORDS: argon; carbon tetrafluoride; Greenspan viscometer; hexafluoroethane; methane; nitrogen; propane; sulfur hexafluoride; viscosity.

1. INTRODUCTION

The semiconductor processing industry requires accurate values of the thermodynamic and transport properties of "surrogate" gases and process

[1] Process Measurements Division, Chemical Science and Technology Laboratory, National Institute of Standards and Technology, Gaithersburg, Maryland 20899-8360, U.S.A.
[2] To whom correspondence should be addressed. E-mail: john.hurly@nist.gov
[3] Current address: P.O. Box 307, Orcas, Washington 98280-0307, U.S.A.

0195-928X/03/1100-1441/0 © 2003 Plenum Publishing Corporation

gases for calibrating mass flow controllers used in process streams. The surrogate gases (e.g., Ar, N_2, SF_6) are benign; however, many of the process gases (e.g, trimethyl-gallium, silane, phosphine) are difficult to handle because they are toxic or highly reactive. Consequently, the thermophysical properties of many process gases have not been accurately measured. To obtain accurate measurements for the process gases efficiently and safely, NIST has developed small, robust, acoustic resonators that require only small samples and that can easily be contained within a purged gas cabinet similar to the previously described system used for speed-of-sound measurements [1]. Here, we describe a Greenspan acoustic viscometer and report results obtained with it for seven benign gases (Ar, CH_4, C_3H_8, N_2, SF_6, CF_4, C_2F_6).

In 1953 Greenspan and Wimenitz [2] proposed determining the viscosity of gases by measuring the energy losses in a double Helmholtz acoustic resonator. We implemented their proposal by building a double Helmholtz resonator [3–5] composed of two gas-filled cylindrical chambers of radius r_c and length L_c that were coupled by a duct of radius r_d and length L_d. (See Fig. 1.) In the Helmholtz mode, the gas within the resonator oscillates between the two chambers through the duct. Most of the energy in the oscillation is dissipated by viscous friction, either within the duct or within a distance of order r_d outside the ends of the duct. In this respect, the Greenspan viscometer resembles an oscillating version of a capillary viscometer.

For the resonator in Fig. 1, the Helmholtz resonance occurred near the frequency $f_0^2 \approx (cr_d)^2/(2\pi L_d V_c)$, where c is the speed of sound and V_c is the volume of one chamber [3]. In the vicinity of f_0, we measured the frequency dependence of the in-phase and quadrature voltages at the source and detector transducers. The complex ratio (detector voltage)/(source voltage) $\equiv \hat{W} = u + iv$ is proportional to the ratio of the acoustic pressure in the chamber to the acoustic source strength and defines the frequency response of the oscillating gas at the measurement frequency. The frequency dependence of $\hat{W}$ was analyzed to determine the speed of sound and the viscosity of the gas. This could be done very precisely because f_0 was well below the frequencies of all the other acoustic modes of the enclosed gas and all of the elastic modes of the resonator's body. When the quality factor of the resonance $Q \gg 1$, the complex voltage ratio is well approximated by a Lorentzian function of the frequency (characterized by a resonance frequency, a half-width, and a complex amplitude) plus a background term,

$$\hat{W}(f) = u + iv \approx \frac{\bar{A}}{f - (f_0 + ig)} + \bar{B} + \bar{C}f \tag{1}$$

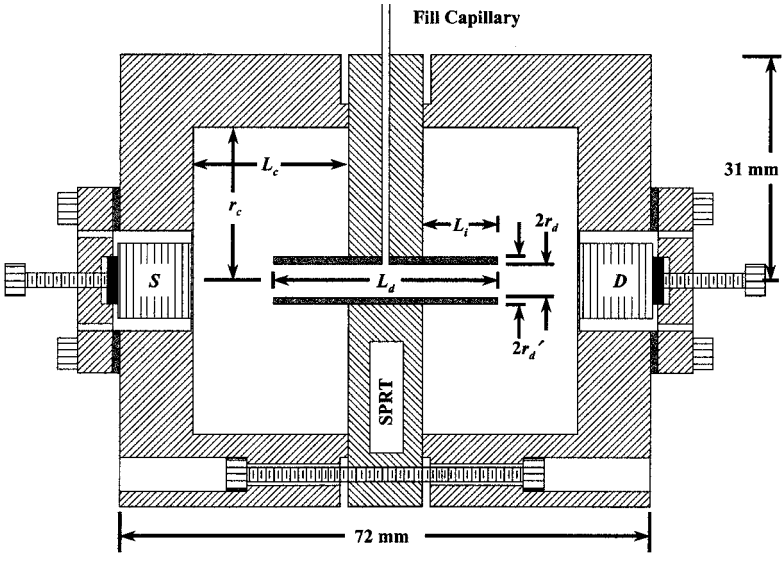

Fig. 1. Cross section of a cylindrical Greenspan viscometer showing two cylindrical chambers connected by a cylindrical duct. Each chamber has a thin diaphragm at the top of the cavities which contain the source (S) and detector (D) transducers. The dimensions in millimeters are $L_d = 31.17$, $r_d = 2.316$, $r_d' = 3.21$, $r_c = 21.02$, $L_c = 21.04$, and $L_i = 10.5$. The fill capillary has an inner radius of 0.10 mm and a length of 80 mm. The viscometer is located inside of a pressure vessel (not shown) filled with argon gas at a pressure equal to that of the sample gas.

where $\bar{A}$, $\bar{B}$, and $\bar{C}$ are complex constants. Here, g is the half-width of the resonance peak at $1/\sqrt{2}$ times its maximum amplitude, and the quality factor is defined by $Q \equiv f_0/(2g)$. Considering only viscous dissipation in the duct, the viscosity η of the gas is related to Q through

$$\eta \approx \pi f_0 \rho (r_d/Q)^2 \tag{2}$$

where ρ is the gas density. Heat transport between the oscillating gas and the metal parts of the resonator causes significant energy dissipation; therefore, Eq. (2) overestimates η. The overestimate is, fractionally $0.44(\gamma-1)/\sqrt{\mathrm{Pr}}$. Here, $\gamma \approx C_p/C_v$ is the ratio of heat capacities, $\mathrm{Pr} \equiv \eta C_p/\lambda$ is the Prandtl number, λ is the thermal conductivity, and the numerical factor 0.44 applies to the specific viscometer shown in Fig. 1. It follows that the uncertainty of the viscosity deduced from the Greenspan viscometer is *at least* $0.22(\gamma-1)/\sqrt{\mathrm{Pr}}\,(\Delta\lambda/\lambda)$ where $(\Delta\lambda/\lambda)$ is the fractional uncertainty of

the thermal conductivity of the gas. As the critical point is approached, $(\gamma-1)/\sqrt{\mathrm{Pr}}$ increases greatly; eventually, the thermal dissipation exceeds the viscous dissipation. Therefore, the Greenspan viscometer is not a useful viscometer near critical points.

In practice, we did not use the approximate relationships, Eqs. (1) and (2). Instead, we determined the viscosity by fitting the frequency-dependent complex-voltage ratio $\hat{W}(f)$ with the theoretical function (Eq. (36) in Ref. 4) derived by Gillis et al. from a detailed acoustic model. This model accounts for thermal and viscous energy dissipation everywhere on the resonator's boundaries and also for the attenuation of sound throughout the volume of gas in the resonator. The model acoustic response function reduces to the Lorentzian form in the limit $Q \gg 1$; however, the more general function is necessary to exploit the high precision of the Greenspan viscometer over the entire range of experimental conditions. Some important aspects of the model are discussed in Section 3.

The primary improvement in this work over that of Wilhelm et al. [5] is the use of a more accurate model. We also improved the corrosion resistance and interior surface finish of the resonator by using diaphragms that were integral parts of the resonator walls instead of disks that were soldered in place. These improvements permitted us to replace the *ad hoc* calibration function used in Ref. 5 with a physically-motivated fit of a single parameter that characterizes the dissipation in the divergent acoustic flow at each end of the duct. As in Ref. 4, this parameter was obtained by comparing the present measurements with helium in the viscometer to reference data on one isotherm ($T = 298.15$ K; 0.6 to 3.4 MPa). The reference value of the zero-density viscosity was taken from the *ab initio* calculations of Hurly and Moldover [6], and the density dependence of the viscosity was taken from the measurements of Kestin et al. [7]. The deviations of the helium viscosity results before and after calibration are shown in Fig. 2.

Below, we present results for the viscosity in five other well-studied gases: Ar, CH_4, C_3H_8, N_2, and SF_6. These gases were used to test our understanding of the acoustic model and the performance of the Greenspan viscometer. Over the entire pressure range, all of the present measurements fall within $\pm 0.5\%$ of previously published measurements obtained using other experimental techniques. In the limit of zero density, our measurements fall within $\pm 0.4\%$ of previously published measurements, which is consistent with their combined uncertainties.

We also report measurements for CF_4 and C_2F_6, two surrogates for process gases whose viscosities had not been accurately measured earlier. For these gases, the viscosity data span the temperature range 210 to 375 K and pressures up to 3.3 MPa. The average uncertainty of the viscosity was 0.42% for CF_4 and 0.55% for C_2F_6. The largest uncertainty (1.9%)

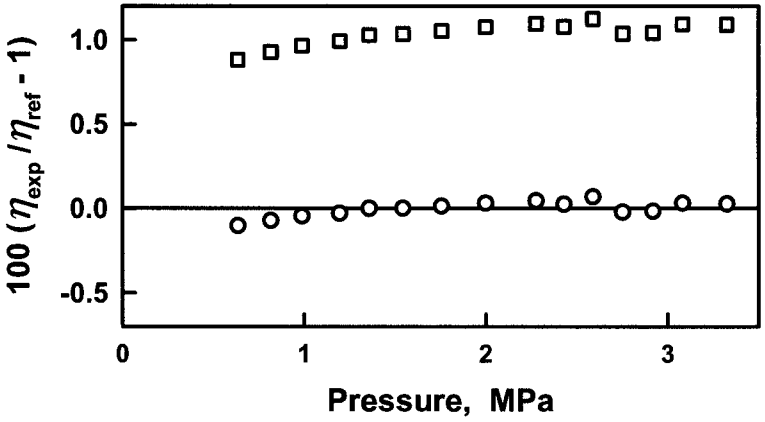

Fig. 2. Deviations of the measured viscosity of helium from reference values before (□) and after (○) calibration. Calibration of the viscometer was achieved by adjustment of two model parameters that describe the effects of diverging-converging flow near the duct ends. The 1% decrease of the viscosity was achieved by a 4% increase in ϵ_r from its calculated value. The second parameter only affected sound speed.

occurred in CF_4, at the highest density (2746 mol·m^{-3}). Of the 1.9%, 0.63% resulted from the 2% uncertainty of the zero-density thermal conductivity of CF_4, reported in the literature.

2. APPARATUS AND EXPERIMENTAL TECHNIQUES

2.1. Resonator

Figure 1 shows a schematic cross section of the Greenspan viscometer. Following Wilhelm et al. [5], it was composed of two cylindrical shells that were sealed with indium-coated surfaces to a central disk that contained the main duct. The shells and the disk were machined out of stainless steel. A diaphragm, driven by a piezoelectric-stack transducer (S in Fig. 1) generated sound in one chamber. The resulting pressure oscillations in the second chamber drove a second diaphragm attached to a similar transducer (D in Fig. 1) used as a detector. Both diaphragms were between 0.10 and 0.15 mm thick. They were formed by machining cavities into the ends of the chambers, leaving only a thin metal wall. This contrasts with the resonator in Ref. 5, which had the diaphragms soldered in place so that the sample gas was in contact with a bead of solder and a seam. Each transducer was pressed against the outer side of a diaphragm by a screw that was supported in a 5 mm thick backing plate.

The duct was an electro-polished section of stainless steel tubing welded in place. We measured the duct's inside radius $r_d = (2.3163 \pm 0.0005)$ mm using a coordinate measuring machine. The ends of the duct had been cut with an electron-discharge machine to produce sharp, right-angled surfaces that facilitated measuring the dimensions of the duct. In hindsight, it would have been wiser to use a duct with rounded, well characterized ends because the acoustic dissipation is particularly sensitive to geometric imperfections (such as burrs or chamfers) near the right-angled ends of the duct than to geometric imperfections elsewhere. This happens because the acoustic velocity increases whenever sharp, external corners are approached. (In the limit of vanishing viscosity, the velocity diverges weakly at external corners.) If the shape of a corner were to change (for example, by the deposit of particles or an oil film), the response function of the viscometer would change.

A capillary tube was used to evacuate the resonator and fill it with test gases. The capillary had an inner radius of 0.10 mm and a length of 80 mm. As shown in Fig. 1, the fill capillary was located at the middle of the duct where the Helmholtz mode has a pressure node because of the resonator's symmetry. At this unique location, there is no oscillatory pressure to drive sound into the capillary [4, 5]. Therefore, the presence of the fill capillary has negligible effects on the resonator's frequency response.

The frequency of the Helmholtz mode f_0 varied from 104 Hz (SF_6 at 298.15 K and 0.15 MPa) to 948 Hz (helium at 298.15 K and 3.38 MPa). If other resonances in the apparatus accidentally occurred near f_0, they would have interfered with the accurate measurement of the acoustic response. When the measurement frequency was increased well above f_0, we encountered a pair of resonances in the test gas that corresponded to the lowest azimuthal modes of the gas in each chamber of the resonator. These modes occur at approximately 6 times f_0 and caused no problems. When evacuated, the resonator had many structural resonances at 12 kHz and at higher frequencies, again well above f_0. In normal use the resonator was suspended in an argon-filled pressure vessel that was maintained at the same pressure as the test gas inside the resonator. Near 300 K, the argon in the pressure vessel had a resonance near 500 Hz and others at much higher frequencies. The 500 Hz mode did not coincide with the Helmholtz mode of the viscometer for any of our test gases. In case of such a coincidence we would have replaced the argon by a gas with a different speed of sound.

Normally, the pressure across the diaphragms separating the test gas from the transducers was maintained in the narrow range $\Delta p = 0.0 \pm 0.5$ kPa. ($\Delta p > 0$ means the argon pressure outside the resonator exceeds the test gas pressure inside the resonator.) With argon as the test gas, we explored the effects of differential pressures up to $\Delta p = \pm 300$ kPa. When

Δp increased, f_0 and the amplitude of the detected voltage increased while g decreased. These changes were reversible, nonlinear functions of Δp. At the extremes, $\Delta p = \pm 300$ kPa, the apparent viscosity changed by $\pm 0.8\%$. In the smaller range, $\Delta p = \pm 50$ kPa, g was a linear function of Δp with a slope equivalent to the pressure-dependent viscosity: $-0.01\ \mu\text{Pa} \cdot \text{s} \cdot \text{kPa}^{-1}$. In the normal operating range, $\Delta p = (0.0 \pm 0.5)$ kPa, the apparent viscosity change was less than $\pm 0.005\%$.

2.2. Pressure and Temperature Measurements

The resonator was suspended vertically inside an argon-filled pressure vessel. Both the fill capillary and the pressure vessel were connected to a Monel[4] gas handling manifold. The test gas was separated from the argon by a high-precision differential pressure gauge (DPG) with a full scale range of ± 13.3 kPa. A pressure controller adjusted the argon pressure to balance the test gas pressure as indicated by a zero output from the DPG. The argon pressure was measured by a quartz Bourdon-tube pressure gauge with a maximum working pressure of 3400 kPa. The uncertainty of the pressure of the test gas was estimated to be ± 0.2 kPa.

A standard platinum resistance thermometer (SPRT) was calibrated on ITS-90 and inserted into a well in the central disk of the resonator opposite to the fill capillary. (See Fig. 1.) The SPRT was connected to a four-wire, high precision 7½-digit multimeter. The uncertainty of the temperature of the test gas was estimated to be 10 mK. The entire pressure vessel was immersed in a thermostated liquid bath. Oil was used as the heat transfer fluid at or above 300 K; methanol was used below 300 K. The bath temperature was monitored by a thermistor and maintained with a PID controller to within 3 mK of the set point.

2.3. Measurement Procedures

At each temperature and pressure, the complex frequency response of the resonator was measured at 22 uniformly spaced frequencies spanning $\pm 2g$ about the resonance frequency f_0 of the Helmholtz mode. At each of the 22 frequencies, a sinusoidal signal was generated by a frequency synthesizer and amplified to drive the source transducer. Two lock-in amplifiers were used to measure the complex voltages at the source and at

[4] In order to describe materials and experimental procedures adequately, it is occasionally necessary to identify commercial products by manufacturer's name or label. In no instance does such identification imply endorsement by the National Institute of Standards and Technology, nor does it imply that the particular product or equipment is necessarily the best available for the purpose.

the detector. At each frequency, the complex voltage ratio $\hat{W}(f)$ was computed and stored as primary data. Noise in the vicinity of the odd harmonics of the power-line frequency (60 Hz) was avoided by omitting measurements within ± 2 Hz of these frequencies.

The source transducer was driven at voltages between 5 and 170 V_{pp} (volts peak-to-peak). We selected the drive voltage using the procedure of Wilhelm et al. [5] to ensure that the transducers, the electronics, and the acoustic flow were all operating in linear regimes. At the highest pressure, the drive voltage was increased until the onset of nonlinearity was detected by an apparent decrease in the Q, as determined by fitting the acoustic model to the detected voltage-vs-frequency data. The voltage was reduced $\sim 25\%$ below that where the nonlinear behavior was observed. As the pressure on the isotherm was reduced, the voltage was increased in proportion to $p^{-1.5}$, thereby, keeping the Reynolds number Re approximately constant. (In steady flow in a circular pipe, the condition $\mathrm{Re} < 2300$ is usually sufficient to ensure laminar flow; however, this condition can be significantly relaxed for oscillating flows [8].)

Typical voltages at the detector ranged from 10 to 40 μV_{pp}. The lock-in amplifier was programmed to measure the real and imaginary voltage components approximately 400 times during 8 s and to return the mean values and their standard deviations. After each frequency change, the lock-in amplifier was allowed to settle for a time that depended on the filter settings. With a time constant set at 0.3 s and a filter slope of 24 dB/octave, a delay of 4.5 s was used. At each frequency, the complex voltage ratio $\hat{W}(f)$ was measured twice, once as the frequencies were scanned upward and again as they were scanned downward, resulting in 44 values of $\hat{W}(f)$. Scanning up and down through the resonance provides redundant data that were used to check their reproducibility. Averaging the up and down data greatly reduces the effects of small temperature drifts.

Each data file contained measurements of the temperature and pressure made just before and just after the scans through the resonance as well as the 44 values of $\hat{W}(f)$. Each data file was analyzed with the model discussed in the next section to calculate the viscosity and speed of sound.

On each isotherm, the resonator was manually loaded with the test gas to the highest pressure while the argon pressure in the surrounding vessel was adjusted continuously to balance the DPG. After the resonator was loaded, the apparatus was operated completely under computer control. Whenever gas was added to or removed from the resonator, adiabatic heating or cooling produced a temperature difference between the resonator and the stirred liquid bath that took approximately 30 minutes to subside to a few millikelvin. Three independent measurements of the frequency response of the resonator were made at each temperature and

pressure, and the data were stored in three files. The independent files were used to estimate the repeatability of the $\eta(T, p)$ results. After the measurements at each pressure were completed, the pressure was reduced by opening and closing valves under computer control and the equilibration and measurement cycles were repeated.

3. RESONATOR MODEL

We analyzed our $\hat{W}(f)$ data using the acoustic response function for the Greenspan viscometer derived by Gillis et al. [4]. Their detailed acoustic model accounts for: (1) viscous boundary losses in the duct, (2) the effects of the convergent-divergent flows at each end of the duct, (3) thermal losses at the gas-resonator boundary, and (4) attenuation of sound throughout the volume of the gas (such as the attenuation caused by translation-vibration relaxation or by density fluctuations near the critical point). Each of these mechanisms contributes to $\hat{W}(f)$ and must be included in the model in order to determine the viscosity accurately. Here, we provide approximate expressions for the frequency response; the full expressions are found in Ref. 4.

When the dissipation is small, e.g., at high pressures or high frequencies, the frequency response is Lorentzian [Eq. (1)] and characterized by the inverse quality factor $Q^{-1} = 2g/f_0$. Approximately, Q^{-1} is the sum of three terms

$$\frac{1}{Q} \approx \frac{1}{Q_v} + \frac{1}{Q_t} + \frac{1}{Q_b} \tag{3}$$

where Q_v^{-1} and Q_t^{-1} are the contributions from viscosity and thermal conduction at the resonator wall, respectively, and Q_b^{-1} is the "bulk" contribution from attenuation throughout the gas-filled volume.

In the low dissipation approximation, the energy loss due to viscosity is

$$\frac{1}{Q_v} = \frac{\delta_v}{r_d} \frac{L_d + 2\epsilon_r r_d}{L_d + 2\delta_i} \tag{4}$$

where $\delta_v \equiv [\eta/(\pi f \rho)]^{1/2}$ is the characteristic distance from the duct wall over which the dissipation occurs. The ratio on the far right of Eq. (4) is approximately 1.04. It accounts for the converging-diverging acoustic flow near both ends of the duct. In the numerator, the geometry-dependent parameter ϵ_r accounts for additional dissipation just inside and just outside the ends of the duct. The value of ϵ_r is sensitive to the detailed shape of the

duct's ends [9, 10]. These details were not measured accurately; instead, ϵ_r was fit to the helium data (Section 4). In the denominator, the geometry-dependent parameter $\delta_i \approx 0.655\, r_d$ accounts for the kinetic energy of the converging-diverging flow.

The contribution to Q^{-1} resulting from the oscillatory heat conduction between the test gas and the chambers' walls is approximately

$$\frac{1}{Q_t} \approx \frac{(\gamma-1)\,\delta_t S_c}{2V_c(1+\chi_t)}. \tag{5}$$

Here, $\delta_t \approx [\lambda/(\pi f \rho C_p)]^{1/2}$ is the exponential decay length for the acoustic temperature difference between the gas and the chamber wall; λ is the thermal conductivity; S_c is the surface area of one chamber; and V_c is the volume of one chamber. In Eq. (5), the parameter $\chi_t \approx [(\rho C_p \lambda)_{gas}/(\rho C_p \lambda)_{solid}]^{1/2}$ accounts for the penetration of the acoustic temperature oscillations into the solid walls of the resonator. In this work, χ_t was always less than 0.01. We included χ_t in the full data analysis; however, we ignore it in the present discussion. The dissipation from heat conduction can be expressed as a correction $\Delta\eta_\lambda$ to the approximate viscosity η given by Eq. (2). Neglecting the end corrections, the fractional correction $\Delta\eta_\lambda/\eta$ is

$$\frac{\Delta\eta_\lambda}{\eta} \approx -\frac{2Q_t^{-1}}{Q_v^{-1}} \approx -\frac{(\gamma-1)\,S_c r_d}{V_c\sqrt{\mathrm{Pr}}} \approx -(0.44)\frac{(\gamma-1)}{\sqrt{\mathrm{Pr}}}. \tag{6}$$

The ratio Q_v/Q_t depends upon the geometry of the particular resonator $[S_c r_d/(2V_c) \approx 0.22]$ and the combination of properties $(\gamma-1)/\sqrt{\mathrm{Pr}}$ of the test gas. The quantity $(\gamma-1)/\sqrt{\mathrm{Pr}}$ must be estimated to interpret the data from the Greenspan viscometer, and the uncertainty of the estimate contributes to the uncertainty of the viscosity, as discussed in Section 5.

Dissipation throughout the volume of the test gas is usually negligible. When it is not, the dissipation throughout the volume can be described by the "bulk" viscosity η_b, which is sometimes called the volume viscosity, dilational viscosity, or second viscosity. Approximately, the contribution of the bulk viscosity to Q^{-1} is

$$\frac{1}{Q_b} = \frac{\omega\eta_b}{\rho c^2} \tag{7}$$

and the correction to the apparent viscosity is

$$\frac{\Delta\eta_b}{\eta} \approx -\frac{2Q_b^{-1}}{Q_v^{-1}} \approx -(k_0 r_d)\left(\frac{\eta_b}{\eta}\right)^{1/2}\left(\frac{2k_0\eta_b}{pc}\right)^{1/2} \tag{8}$$

where the inverse length $k_0 \equiv 2\pi f_0/c \approx 5.8\ \mathrm{m}^{-1}$. The bulk viscosity cannot be neglected very near the liquid-vapor critical point of any gas, nor can it be neglected at low densities for certain polyatomic gases (e.g, CH_4, CO_2, Cl_2). These polyatomic gases have symmetries such that many intermolecular collisions are required for their internal degrees of freedom to equilibrate with their translational degrees of freedom. Often, this equilibration is dominated by binary collisions and it can be characterized by a single relaxation time τ_{rel} such that $\tau_{\mathrm{rel}} \propto \rho^{-1}$. Under these conditions, the bulk viscosity is approximately [4]

$$\eta_{\mathrm{b}} = (\gamma - 1)\,\rho c^2 \frac{C_{\mathrm{rel}}}{C_{\mathrm{p}}} \frac{\tau_{\mathrm{rel}}}{1 + (\omega\tau_{\mathrm{rel}})^2} \tag{9}$$

where C_{rel} is the heat capacity of the slowly relaxing vibrational degrees of freedom. In this work, the largest value of $Q_{\mathrm{v}}/Q_{\mathrm{b}}$ was 0.0014 (methane at $T = 293.15\mathrm{K}$ and $p = 120\ \mathrm{kPa}$). Thus, even in the worst case, the bulk viscosity correction to the apparent viscosity was less than 0.3%.

4. CALIBRATION

4.1. Viscosity

Figure 2 shows the significant improvement obtained by calibrating the present Greenspan viscometer with helium at 298.15 K and at pressures from 0.6 to 3.3 MPa. (Below, we show that the same calibration yielded satisfactory results with other gases.) For the calibration, we measured the frequency response $\hat{W}(f)$ of the helium-filled viscometer and we analyzed the data using the full theoretical model to obtain values for both the viscosity and the speed of sound. The analysis required a value for the parameter ε_{r} that characterizes the dissipation in the divergent acoustic flow at the ends of the duct. For a duct with right-angled ends, numerical modeling predicts $\varepsilon_{\mathrm{r}} = \varepsilon_{\mathrm{r0}} - 0.348(\delta_{\mathrm{v}}/r_{\mathrm{d}})^{1/3} + 1.15(\delta_{\mathrm{v}}/r_{\mathrm{d}})$ with $\varepsilon_{\mathrm{r0}} = 0.987$. As described in Ref. 4, $\varepsilon_{\mathrm{r0}}$ was increased to $\varepsilon_{\mathrm{r0}} = 1.03$ to better fit reference data for the viscosity of helium. For reference data, we used *ab inito* values for the zero-density viscosity (0.06% uncertainty) and the zero-density thermal conductivity [6]. We also used the *ab inito* values for the second virial coefficient to calculate ρ, C_{p}, and c at each temperature and pressure. We took the density dependence of the viscosity and the thermal conductivity from Kestin and Leidenfrost [11] and from Kestin et al. [7], respectively. We included the small contribution to the equation of state from the third virial coefficient $C(T)$, taken from a fit to experimental results [12].

At helium pressures below 0.6 MPa, the Q was less than 20 and we did not trust the fits to $\hat{W}(f)$ because the fits with $\bar{C}=0$ and $\bar{C}\neq 0$ yielded viscosities that differed by 1% or more. Thus, data with $p<0.6$ MPa were not used for the calibration.

4.2. Speed of Sound

The present Greenspan viscometer was not designed to determine accurately the speed of sound in test gases. However, after a simple calibration, the deviations of c from reference values were less than $\pm 0.04\%$ for all five reference gases studied. We had hoped to determine c from the dimensions of the resonator that we measured prior to assembling it. However, as described in Ref. 4, adjusting the parameter ε_i from the value $\varepsilon_i=0.86$ calculated in Ref. 10 to the value $\varepsilon_i=0.96$ improved the fit to the speed-of-sound data, particularly for helium at low densities. The parameter ε_i accounts for the kinetic energy of the divergent flow at the duct's ends, and its value is sensitive to hard-to-measure details of the duct's end. We emphasize that the adjustment of ε_i had a negligible effect on the viscosity. The thermal expansion of 316 stainless steel ($1.7\times 10^{-5}\,\mathrm{K}^{-1}$) was used to adjust the dimensions of the resonator from the values measured at 20°C.

After calibration, the fractional deviations of the present speed of sound from reference data were less than 0.04% [Figs. 3b and 5b]. For helium, argon, and nitrogen, the deviations have a remarkably simple pressure dependence: $(c_{\text{experiment}}/c_{\text{reference}})-1\approx -10^{-4}p/\text{MPa}$. [4] This dependence may be a consequence of the finite compliance of the resonator, which is not included in our model. The deviations for SF_6 have a complex pressure dependence. In part, this may reflect the difficulties of making accurate equation-of-state and speed-of-sound measurements near the saturated vapor pressure. If not accounted for, precondensation will reduce the apparent speed of sound and increase the dissipation of energy because of increased oscillatory heat transfer at the gas-solid boundary [13].

5. UNCERTAINTIES

The kinematic viscosity η/ρ was determined by fitting the $\hat{W}(f)$ data by the model for the viscometer (Eq. (36) of Ref. 4). The model requires, as inputs: the dimensions of the resonator and certain properties of the test gas (γ, λ/C_p, and, in a few cases, the bulk viscosity, η_b) at the experimental temperature and pressure. The free parameters in the fit are the kinematic viscosity η/ρ, the speed of sound c, a complex amplitude $\bar{A}$, and either one or two complex constants representing the complex background $\bar{B}+\bar{C}f$.

The model was fit to the $\hat{W}(f)$ data with weights determined by the standard deviations of the measured signal at each frequency; however, the uncertainties of η/ρ and c are much larger than those determined by the fitting program. To discuss the uncertainties, we group them by their four sources: (1) the instruments, (2) imperfections of the model of the resonator, (3) estimates of $(\gamma-1)/\sqrt{\mathrm{Pr}}$ of the test gas, and (4) minor contributions from the dimensional measurements and from other gas properties including the density ρ, which is required if η is to be determined from η/ρ.

The estimated uncertainty in the measured temperature with the SPRT is 10 mK. The estimated uncertainty in pressure measurements is typically less than 0.2 kPa. For each gas in the range studied, the viscosity $\eta(T, p)$ depended only weakly on temperature and pressure. Thus, the imperfect specification of the state of the gas had a negligible effect on the results. At low pressures, the relative uncertainty of the pressure is $200\ \mathrm{Pa}/p$. This pressure uncertainty propagates into a density uncertainty *via* the equation of state and then into a marginally significant viscosity uncertainty *via* Eq. (2).

The measurement of the voltage ratio $\hat{W}(f)$ leads to uncertainties that increase as the pressure is reduced. With decreasing pressure, the detected signal decreases and the Helmholtz mode is spread over a wider frequency range ($Q \propto p^{1/2}$, unless the bulk dissipation is significant) and the fitted viscosity becomes increasingly sensitive to phenomena that are not included in the model. These include: (1) other resonances, (2) frequency dependences of the transducers and the electronics, and (3) possible crosstalk between the transducers. The background terms in the fitting function [$\bar{B}+\bar{C}f$ in Eq. (1)] compensate for linear frequency dependences of the transducers, crosstalk, etc.; however, more complicated frequency dependences will yield systematic errors in the fitted viscosity. Typically, we rejected data when the fitted viscosity changed by more than 1% upon deleting the constant $\bar{C}$ from the fitting function. Usually this occurred when $Q \lesssim 30$.

The viscometer was calibrated using the viscosity of helium as determined by *ab initio* calculations [6]. If we had calibrated the viscometer using the viscosity of argon from Ref. [14], the viscosity results reported here would be essentially unchanged at zero density, and they would be reduced by approximately 0.3% at the highest densities.

Equation (6) implies that the viscosity deduced from the Greenspan viscometer will have an uncertainty contribution from estimating the ratio $(\gamma-1)/\sqrt{\mathrm{Pr}}$ for the test gas. For all the gases we have studied, $(\gamma-1)$ is well known, often from speed-of-sound measurements. However, the ratio λ/C_{p}, which appears in the Prandtl number, does contribute to the

uncertainty of the viscosity. Often, C_p is also well known from speed-of-sound measurements; in such cases, we are still concerned with the uncertainty of the thermal conductivity. We provide three examples of the effects of a 2% uncertainty of the thermal conductivity ($\Delta\lambda/\lambda = 0.02$). For helium or argon at low density, $\Delta\lambda/\lambda = 0.02$ leads to a 0.36% uncertainty of the viscosity. For CF_4, $\Delta\lambda/\lambda = 0.02$ leads to uncertainties from 0.07% to 0.62% of the viscosity, and the largest value occurs at the highest density (2746 $mol \cdot m^{-1}$, 225 K, 3.1 MPa). Finally, for C_2F_6, $\Delta\lambda/\lambda = 0.02$ leads to uncertainties from 0.04 to 0.22% of the viscosity. We note that one can design a Greenspan viscometer that is less sensitive to the thermal conductivity of the test gas by reducing $S_c r_d/(2V_c)$. However, such an instrument would be less compact and/or have a more complicated structure and/or operate with a smaller Q.

Because we calibrated the viscometer with helium at 298 K, the results for other gases and at other temperatures are very insensitive to the dimensional measurements. Additional uncertainties result from calculating the gas density and the heat capacity C_p from equations of state. For each gas, we specify the equation of state used in the analysis. If a better equation of state becomes available, the viscosity can be recalculated. The purity (as specified by the supplier) of all test gases studied was 0.9999 or higher by mole fraction. The viscosity of gases is insensitive to impurities; however, the measured speed of sound is not. The tabulated speeds of sound agree with values from the literature within 0.04%. This indicates that the gases were not significantly contaminated.

Tables II to VIII include the uncertainty of each viscosity measurement. The tabulated uncertainty includes contributions from the known experimental uncertainties: temperature, pressure, density, heat capacity, thermal conductivity, the quality of the fit of $\hat{W}(f)$, and the scatter among at least three redundant measurements at each temperature and pressure. The uncertainties in density, heat capacity, and thermal conductivity were taken directly from the literature. Each property was changed within its estimated uncertainty, and the viscosity was re-calculated with the full model to determine how the uncertainty propagated into the viscosity. The absolute values of these contributions were added to the contribution from the fit of $\hat{W}(f)$ and the scatter among the redundant measurements. Thus, the tabulated uncertainties are conservative; however, they necessarily rely on uncertainties from the literature.

6. RESULTS

To assess the performance of our viscometer, five reference gases were studied. The viscosities of Ar, N_2, CH_4, C_2H_6, and SF_6 were measured near

room temperature. The viscosity of argon was then measured on three other isotherms up to 373.15 K to search for temperature-dependent problems. None was found; however, the signal at the detector transducer decreased noticeably at the highest temperature. After the viscometer's performance was tested, the viscosities of CF_4 and C_2F_6 were measured throughout the accessible temperature and pressure ranges.

The viscosity data were acquired along isotherms and then fit by the polynomial function of density:

$$\eta(T, p) = \eta_0(T)[1 + B_\eta(T)\,\rho(T, p) + C_\eta(T)\,\rho^2(T, p)] \tag{10}$$

The resulting values of the zero-density viscosity η_0 and the second and third viscosity virial coefficients, B_η and C_η, are listed in Table I. For

Table I. Coefficients for Eq. (10)

Gas	T (K)	$\eta_0(T)$ (μPa·s)	$B_\eta(T)$ ($cm^3 \cdot mol^{-1}$)	$C_\eta(T)$ ($cm^3 \cdot kmol^{-1})^2$
Ar	293.15	22.31	22.9	2.0
Ar	298.15	22.61	24.2	1.1
Ar	333.15	24.78	24.0	
Ar	348.15	25.67	23.9	
Ar	373.15	27.13	23.0	
CH_4	293.15	10.92	21.7	7.9
N_2	298.15	17.77	14.0	5.1
C_3H_8	298.15	8.10	−12.1	67.2
SF_6	298.15	15.27	−5.0	76.4
CF_4	210	12.65	4.5	43.8
CF_4	225	13.45	20.7	29.1
CF_4	250	14.74	36.0	19.5
CF_4	275	16.06	32.6	21.4
CF_4	300	17.31	35.8	18.5
CF_4	325	18.54	34.9	20.8
CF_4	350	19.73	34.1	17.7
CF_4	375	20.90	30.0	19.6
C_2F_6	225	10.84	−1.3	
C_2F_6	250	11.92	−3.2	79.7
C_2F_6	275	12.98	30.2	54.4
C_2F_6	300	14.03	41.4	57.8
C_2F_6	325	15.08	44.7	58.5
C_2F_6	350	16.09	51.8	52.9
C_2F_6	375	16.97	72.8	41.1

Ar, CF_4, and C_2F_6, we acquired data on several isotherms; for these gases, we provide a polynomial representation of the zero-density values $\eta_0(T)$.

6.1. Argon

The viscosity of argon was measured along five isotherms spanning the temperatures 293.15 to 373.15 K at pressures up to 3.3 MPa. The results are listed in Table II. The equation of state of Estrada-Alexanders and Trusler [15] was used to calculate the density and C_p at each temperature and pressure. They estimate the uncertainty of their equation of state to be 0.025% for density and 0.1% for C_p. Thermal conductivities were taken from Sun et al. [16] who claims an uncertainty of 1%. Figure 3a shows the deviations of the present viscosities from a fit to the viscosities of Wilhelm and Vogel [14] who used a vibrating wire viscometer. Also shown in Fig. 3a are the viscosities measured by Evers et al. [17] who used a rotating cylinder viscometer. The three sets of measurements are consistent within $\pm 0.5\%$ over the entire range of densities. At the lowest densities, the deviations of our measurements drop more sharply. In this region we suspect that the model for the Greenspan viscometer is beginning to fail as the Q decreases.

To display deviations, we represent our five values of η_0 by the polynomial,

$$\eta_0(T)/\mu\text{Pa}\cdot\text{s} = 0.545 + 8.415\times 10^{-2}\,(T/\text{K}) - 3.73\times 10^{-5}\,(T/\text{K})^2 \qquad (293.15\ \text{K} \leqslant T \leqslant 373.15\ \text{K}) \qquad (11)$$

with a fractional standard deviation of 0.0001. Figure 4a compares the present values of η_0 to Eq. (11) and to previously reported values. Figure 4b expands Fig. 4a using Eq. (11) as the baseline. Our values of η_0 are within 0.1% of the values determined by Wilhelm and Vogel [14], Evers et al. [17], Vogel [18], and Bich et al. [19]. Quantitatively, the fractional differences [(this work)/(literature) − 1] are: −0.0005 at 298.15 K and 0.0003 at 348.15K for Wilhelm and Vogel [14]; −0.0003 at 293.15 K, −0.0001 at 333.15 K, and 0.0001 at 373.15 K for Evers et al. [17]; and −0.0013 at 298.15 K and −0.0003 at 348.15 K for Vogel [18]. The data in Fig. 4 were obtained using diverse methods. We used a Greenspan viscometer; Wilhelm and Vogel [14] used a vibrating wire, Evers et al. [17] used a rotating cylinder, and Vogel [18] used an oscillating disk. Remarkably, the four independent methods yield values of η_0 that agree within their experimental uncertainties. This provides great confidence in the accuracy of the techniques and the reported values for η_0.

Table II. Viscosity (η) and Speed-of-Sound (c) Measurements in Argon[a]

p (kPa)	c ($m \cdot s^{-1}$)	η ($\mu Pa \cdot s$)	p (kPa)	c ($m \cdot s^{-1}$)	η ($\mu Pa \cdot s$)
		$T = 293.15$ K			
3300.4	321.92	23.11 ± 0.08	1552.8	320.07	22.66 ± 0.07
3126.5	321.68	23.05 ± 0.07	1427.3	319.96	22.64 ± 0.06
2962.6	321.50	23.02 ± 0.08	1292.1	319.84	22.60 ± 0.06
2810.2	321.33	22.97 ± 0.08	1170.0	319.77	22.57 ± 0.06
2664.0	321.17	22.93 ± 0.07	1040.0	319.64	22.54 ± 0.05
2525.0	321.02	22.90 ± 0.07	910.0	319.53	22.51 ± 0.05
2392.9	320.88	22.87 ± 0.08	782.8	319.43	22.48 ± 0.05
2267.5	320.75	22.82 ± 0.06	661.9	319.34	22.45 ± 0.06
2110.4	320.60	22.79 ± 0.06	541.0	319.25	22.42 ± 0.06
1963.8	320.45	22.75 ± 0.07	422.7	319.17	22.40 ± 0.06
1827.1	320.32	22.72 ± 0.07	307.4	319.09	22.36 ± 0.08
1699.8	320.21	22.69 ± 0.06			
		$T = 298.15$ K			
3316.2	324.82	23.42 ± 0.06	1471.1	322.81	22.94 ± 0.06
3142.1	324.60	23.36 ± 0.06	1602.9	322.93	22.99 ± 0.06
2976.7	324.40	23.32 ± 0.06	1352.7	322.70	22.92 ± 0.06
2819.5	324.22	23.28 ± 0.06	1222.8	322.58	22.89 ± 0.06
2670.5	324.05	23.24 ± 0.07	1105.0	322.47	22.87 ± 0.06
2529.0	323.89	23.21 ± 0.07	981.9	322.36	22.85 ± 0.06
2394.9	323.74	23.18 ± 0.06	857.6	322.26	22.82 ± 0.06
2267.8	323.61	23.14 ± 0.07	735.2	322.16	22.79 ± 0.06
2147.3	323.48	23.11 ± 0.06	614.3	322.06	22.76 ± 0.06
1996.3	323.32	23.07 ± 0.06	503.1	321.97	22.74 ± 0.07
1855.7	323.18	23.04 ± 0.06	382.3	321.88	22.70 ± 0.06
1724.7	323.05	23.00 ± 0.06	253.7	321.79	22.64 ± 0.07
		$T = 333.15$ K			
3374.5	344.32	25.52 ± 0.07	1492.3	341.73	25.10 ± 0.06
3243.3	344.11	25.49 ± 0.07	1387.6	341.60	25.08 ± 0.06
3116.8	343.93	25.46 ± 0.06	1289.7	341.49	25.06 ± 0.06
2995.1	343.75	25.43 ± 0.07	1176.7	341.35	25.03 ± 0.07
2878.1	343.59	25.41 ± 0.07	1073.6	341.22	25.02 ± 0.06
2765.6	343.43	25.38 ± 0.07	961.6	341.09	24.99 ± 0.06
2657.4	343.28	25.36 ± 0.06	861.3	340.97	24.98 ± 0.06
2553.4	343.14	25.34 ± 0.07	757.1	340.85	24.95 ± 0.06
2453.4	343.00	25.30 ± 0.06	653.5	340.73	24.93 ± 0.07
2310.5	342.80	25.29 ± 0.07	553.6	340.61	24.90 ± 0.06
2175.9	342.61	25.24 ± 0.06	451.9	340.50	24.89 ± 0.06
2049.0	342.45	25.23 ± 0.06	451.9	340.50	24.89 ± 0.06
1929.4	342.29	25.20 ± 0.06	349.1	340.38	24.85 ± 0.07
1816.6	342.15	25.17 ± 0.07	120.0	340.14	24.80 ± 0.07
1710.4	342.01	25.15 ± 0.06	349.1	340.38	24.85 ± 0.07
1610.2	341.89	25.13 ± 0.07	120.0	340.14	24.80 ± 0.07
1492.3	341.73	25.10 ± 0.06			

Table II. *(Continued)*

p (kPa)	c ($m \cdot s^{-1}$)	η ($\mu Pa \cdot s$)	p (kPa)	c ($m \cdot s^{-1}$)	η ($\mu Pa \cdot s$)
		$T = 348.15$ K			
3340.3	352.15	26.39±0.07	1760.7	349.79	26.04±0.06
3205.1	351.92	26.36±0.07	1620.5	349.60	26.02±0.06
3075.7	351.72	26.32±0.06	1496.3	349.43	26.00±0.06
2951.6	351.53	26.30±0.07	1364.2	349.25	25.96±0.06
2774.7	351.27	26.26±0.07	1241.8	349.08	25.93±0.06
2608.2	351.02	26.23±0.06	1109.2	348.91	25.91±0.06
2451.7	350.79	26.18±0.07	990.4	348.75	25.89±0.06
2304.4	350.57	26.17±0.07	867.8	348.58	25.85±0.07
2165.8	350.37	26.12±0.06	746.1	348.43	25.83±0.07
2035.4	350.18	26.10±0.07	617.4	348.26	25.79±0.07
1912.8	350.01	26.07±0.07			
		$T = 373.15$ K			
3335.8	364.84	27.80±0.07	1628.8	362.10	27.46±0.07
3194.6	364.61	27.78±0.07	1498.0	361.91	27.44±0.07
3059.1	364.38	27.74±0.07	1359.3	361.70	27.40±0.07
2929.1	364.16	27.73±0.07	1232.0	361.51	27.38±0.07
2804.7	363.95	27.68±0.07	1094.9	361.31	27.35±0.07
2628.1	363.66	27.67±0.07	972.9	361.13	27.32±0.07
2462.5	363.39	27.63±0.07	847.4	360.95	27.31±0.07
2307.2	363.15	27.60±0.07	723.6	360.78	27.28±0.08
2161.6	362.92	27.56±0.07	605.6	360.61	27.25±0.08
2025.0	362.71	27.55±0.07	487.2	360.45	27.23±0.07
1897.0	362.51	27.51±0.07	369.3	360.29	27.19±0.08
1777.1	362.33	27.49±0.07			

[a] ρ calculated from Ref. 15.

Figure 3b shows the relative deviations of measured speeds of sound. The Greenspan viscometer was not designed to measure the speed of sound. However, this quantity is a good indicator of the quality of the measurements and the purity of the sample gas.

6.2. Methane

The viscosity of methane was measured along the 293.15 K isotherm at pressures up to 3.3 MPa. The results are presented in Table III. The equation of state of Trusler and Zarari [20] was used to calculate the density

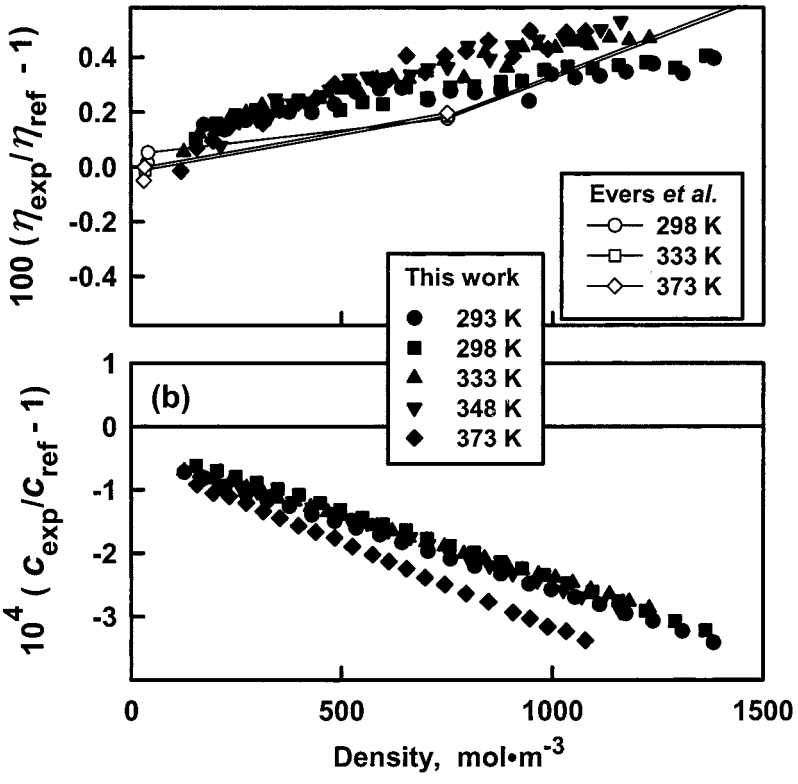

Fig. 3. (a) Fractional deviations of measured viscosities of argon from those of Wilhelm and Vogel [14] as a function of density. Included in the figure are the deviations of the measurements of Evers et al. [17] at 293.15, 333.15, and 373.15 K. (b) Fractional deviations of the speed of sound in argon from Estrada-Alexanders and Trusler [15].

and C_p from the measured temperature and pressure with a claimed uncertainty of 0.02% for density and 0.1% for C_p. Reference 20 also provided the relaxation times required to calculate the bulk viscosity corrections. Thermal conductivities were taken from Younglove and Ely [21] who report an uncertainty of 4%. The isotherm was fit by Eq. (10), and the resulting parameters are listed in Table I. Figure 5a shows that the measured viscosities reproduce the reference values of Vogel et al. [22] to better than 0.2% over all densities. Our zero-density viscosities for methane differ fractionally by 0.0007 from the data of Vogel et al. [22] and by −0.0027 from those of Evers et al. [17]. Figure 5b shows that the measured speeds of sound agree with reference data to within 0.01%.

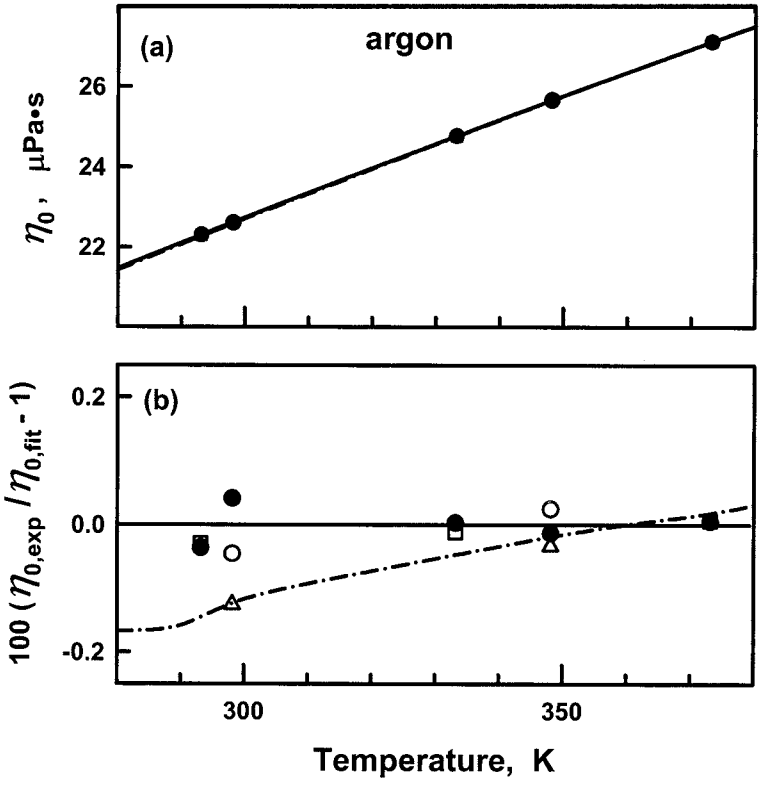

Fig. 4. (a) Zero-density viscosities of argon. The present results (●) are the zero-density intercepts from the fits of Eq. (10) to the isotherms. The solid line is Eq. (11). Also shown are the values of (○) Wilhelm and Vogel [14], (□) Evers et al. [17], (△) Vogel [18], and (–·–) Bich et al. [19]. (b) Fractional deviations from Eq. (11) of the data from the upper figure.

6.3. Propane

The viscosity of propane was measured along the 298.15 K isotherm at pressures up to 830 kPa. The results are listed in Table IV. The equation of state of Span and Wagner [23] was used to calculate density and C_p from the measured temperature and pressure with an uncertainty of 0.02% in density and 0.1% for C_p. Thermal conductivities were taken from Marsh et al. [24] who claim an uncertainty of 2%. The isotherm was fit by Eq. (10), and the resulting parameters are listed in Table I. Figure 5a shows that the measured viscosities agree with the values of Wilhelm and Vogel

Table III. Viscosity (η) and Speed-of-Sound (c) Measurements in Methane[a]

p (kPa)	c ($m \cdot s^{-1}$)	η ($\mu Pa \cdot s$)	p (kPa)	c ($m \cdot s^{-1}$)	η ($\mu Pa \cdot s$)
		$T = 293.15$ K			
3324.0	435.61	11.44±0.06	1633.7	440.02	11.12±0.02
3166.9	436.00	11.41±0.06	1494.6	440.44	11.10±0.05
3009.4	436.36	11.37±0.05	1366.9	440.83	11.08±0.05
2862.1	436.71	11.34±0.05	1227.6	441.26	11.06±0.05
2718.5	437.06	11.31±0.05	1102.0	441.66	11.04±0.05
2580.7	437.40	11.29±0.05	971.3	442.08	11.02±0.04
2449.5	437.74	11.26±0.05	840.3	442.50	11.01±0.04
2324.6	438.07	11.24±0.05	713.6	442.93	10.99±0.05
2167.3	438.50	11.21±0.05	583.9	443.36	10.98±0.04
2020.1	438.91	11.18±0.05	460.4	443.79	10.97±0.05
1882.5	439.30	11.16±0.02	337.0	444.22	10.95±0.04
1753.9	439.67	11.14±0.02	216.6	444.65	10.93±0.05
1633.7	440.02	11.12±0.02	118.2	445.04	10.92±0.05

[a] ρ calculated from Ref. 20.

[14] to within 0.5%, with the zero-density viscosity differing fractionally by 0.0047. Figure 5b shows the deviations of the speed of sound are less than 0.02%.

6.4. Nitrogen

The viscosity of nitrogen was measured along the 298.15 K isotherm at pressures up to 3.3 MPa. The results are listed in Table V. The equation of state of Span et al. [25] was used to calculate density and C_p from the measured temperature and pressure, with a claimed uncertainty of 0.02% in density and 0.01% in C_p. Thermal conductivities were taken from Perkins et al. [26] who report an uncertainty of 1%. Speeds of sound were taken from Estela-Uribe and Trusler [27]. The vibration relaxation time for η_b came from Zuckerwar and Griffin [28]. The isotherm was fit by Eq. (10), and the resulting parameters are listed in Table I. Figure 5a shows the measured viscosities reproduce the reference values of Vogel [18], using the density dependence of Kestin et al. [29], to within 0.2% at all densities, and differing fractionally by 0.0008 at zero density. Figure 5b shows the measured sound speeds agree to 0.02%. In the worst case, the bulk viscosity correction was only 0.0015%.

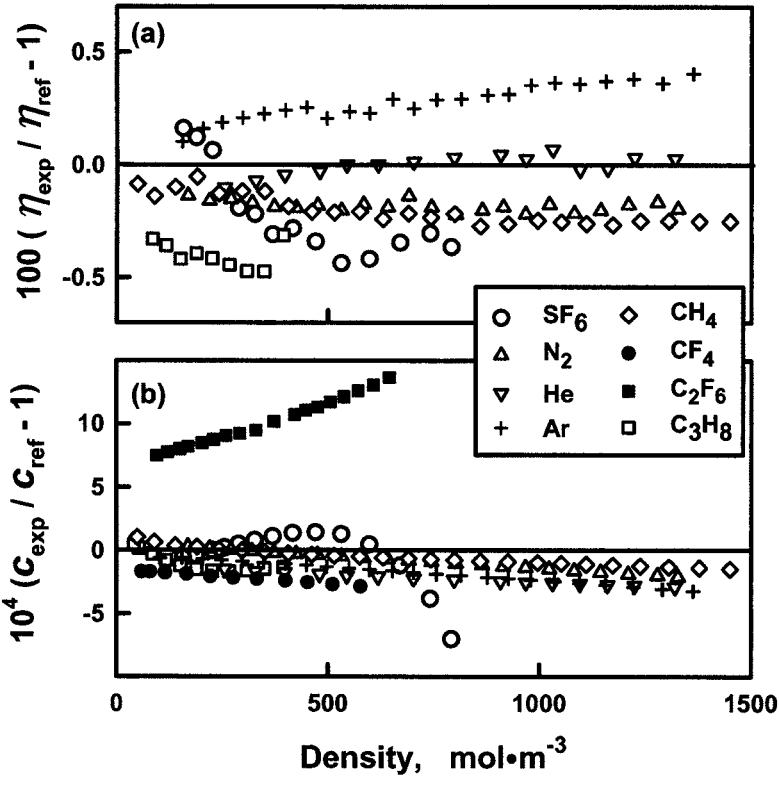

Fig. 5. Fractional deviations of measured viscosities and speeds of sound for T near 300 K from reference values as discussed in Section 6.

Table IV. Viscosity (η) and Speed-of-Sound (c) Measurements in Propane[a]

p (kPa)	c (m·s^{-1})	η (μPa·s)	p (kPa)	c (m·s^{-1})	η (μPa·s)
		$T = 298.15$ K			
830.9	221.29	8.15±0.02	353.8	240.19	8.09±0.02
750.4	224.81	8.12±0.02	277.3	242.83	8.10±0.02
674.3	228.02	8.11±0.02	201.5	245.37	8.10±0.02
594.2	231.26	8.10±0.02	126.1	247.82	8.08±0.02
513.2	234.39	8.10±0.02	99.4	248.68	8.09±0.02
434.3	237.32	8.10±0.02			

[a] ρ calculated from Ref. 23.

Table V. Viscosity (η) and Speed-of-Sound (c) Measurements in Nitrogen[a]

p (kPa)	c ($m \cdot s^{-1}$)	η ($\mu Pa \cdot s$)	p (kPa)	c ($m \cdot s^{-1}$)	η ($\mu Pa \cdot s$)
		$T = 298.15$ K			
3278.3	357.99	18.25±0.03	1709.4	354.78	17.99±0.03
3158.9	357.70	18.24±0.03	1586.4	354.55	17.96±0.03
2988.3	357.32	18.20±0.03	1444.9	354.30	17.95±0.03
2826.8	356.98	18.17±0.03	1315.9	354.07	17.92±0.03
2673.8	356.66	18.14±0.03	1176.2	353.83	17.91±0.03
2528.1	356.39	18.12±0.03	1051.1	353.61	17.89±0.03
2390.7	356.10	18.09±0.03	921.7	353.40	17.87±0.03
2260.8	355.84	18.07±0.03	793.2	353.19	17.86±0.03
2138.0	355.59	18.05±0.03	669.7	352.99	17.84±0.03
1984.4	355.29	18.02±0.03	544.4	352.79	17.83±0.03
1841.8	355.02	18.00±0.03	418.1	352.60	17.81±0.03
1709.4	354.78	17.99±0.03			

[a] ρ calculated from Ref. 25.

6.5. Sulfur Hexafluoride

The viscosity of sulfur hexafluoride was measured along the isotherm at 298.15 K at pressures up to 1.55 MPa. The results are listed in Table VI. The equation of state of Hurly et al. [30] was used to calculate density and C_p from the measured temperature and pressure, with uncertainties of 0.1%. Zero-density thermal conductivities were taken from Zherdev et al. [31] who report an uncertainty of 3%. The density dependence of the thermal conductivity was taken from the extended corresponding states model of McLinden et al. [32], who do not estimate their uncertainty. The isotherm was fit by Eq. (10), and the resulting parameters are listed in Table I. As reference data for the viscosity of SF_6, we took the results of Timrot et al. [33] who claim an uncertainty of 0.7%. Our value of η_0 is only 0.5% above the reference value and only 0.24% above the value of η_0 from Strehlow and Vogel [34]. Figure 5a shows the deviations from the reference values.

Figure 5b compares the present speeds of sound with those in Ref. 30. They agree within 0.03%; however, the abrupt downward trend in the present data above 500 $mol \cdot m^{-3}$ suggests the onset of precondensation [13].

Table VI. Viscosity (η) and Speed-of-Sound (c) Measurements in SF_6[a]

p (kPa)	c ($m \cdot s^{-1}$)	η ($\mu Pa \cdot s$)	p (kPa)	c ($m \cdot s^{-1}$)	η ($\mu Pa \cdot s$)
		$T = 298.15$ K			
1558.1	112.52	15.94±0.07	738.6	126.33	15.37±0.04
1481.7	113.97	15.87±0.07	660.9	127.46	15.34±0.04
1368.6	116.06	15.75±0.07	590.8	128.47	15.33±0.04
1248.0	118.20	15.64±0.05	527.5	129.36	15.33±0.05
1130.7	120.20	15.55±0.05	444.3	130.50	15.32±0.06
1020.1	122.00	15.49±0.04	373.6	131.46	15.30±0.04
917.8	123.62	15.44±0.04	295.9	132.50	15.25±0.06
824.0	125.06	15.39±0.04			

[a] ρ calculated from Ref. 30.

6.6. Carbon Tetrafluoride

The viscosity of carbon tetrafluoride was measured along eight isotherms between 210 and 375 K, at pressures up to 3.3 MPa. Table VII lists the results. The equation of state of Hurly [1] was used to calculate the density and C_p from the measured temperature and pressure with uncertainties of 0.1%. Thermal conductivities were taken from Uribe et al. [35] who claim an uncertainty of 2%, with the density dependence taken from Ref. 32. Each isotherm was fit by Eq. (10), and the results are listed in Table I. To display deviations, we represent our eight values of η_0 for CF_4 by the polynomial,

$$\eta_0(T)/\mu Pa \cdot s = 0.309 + 6.358 \times 10^{-2}\,(T/K) - 2.31 \times 10^{-5}\,(T/K)^2$$
$$(210\ K \leqslant T \leqslant 373\ K) \qquad (12)$$

with a fractional standard deviation of 0.0004. Figure 6a shows the viscosity as a function of temperature, and Fig. 6b shows the relative deviations from Eq. (12). Also shown are the previously published measurements of the viscosity of CF_4 [36–41, 43]. The scatter in the previously published values is about 2%, the present values are accurate to within 0.5%, significantly reducing the uncertainty in the viscosity of this fluid.

Figure 5b compares the present speed-of-sound data at 300 K with the speed-of-sound data that one of us (JJH) reported in Ref. 1. Where the data sets overlap (up to 600 $mol \cdot m^{-3}$), they agree within 0.03%, and similar agreement was obtained on the other isotherms. However, significant differences exist between the present results and those obtained by *extrapolating* the virial equation of state from Ref. 1 to higher densities. At

Table VII. Viscosity (η) and Speed-of-Sound (c) Measurements in SF_4[a]

p (kPa)	c ($m \cdot s^{-1}$)	η ($\mu Pa \cdot s$)	p (kPa)	c ($m \cdot s^{-1}$)	η ($\mu Pa \cdot s$)
		$T = 210$ K			
1319.1	136.15	13.16±0.10	615.7	146.88	12.76±0.07
1241.2	137.45	13.12±0.09	537.3	147.95	12.73±0.06
1159.9	138.77	13.05±0.09	468.2	148.87	12.72±0.06
1075.0	140.12	12.98±0.09	388.8	149.92	12.71±0.07
992.1	141.42	12.89±0.08	307.4	150.98	12.69±0.06
912.9	142.63	12.87±0.08	231.2	151.95	12.67±0.07
838.3	143.72	12.84±0.07	157.6	152.87	12.65±0.06
768.6	144.72	12.80±0.07	124.0	153.29	12.65±0.15
704.0	145.65	12.79±0.07			
		$T = 225$ K			
2316.5	131.07	15.05±0.31	988.9	148.80	13.73±0.08
2218.6	132.61	14.92±0.29	901.3	149.80	13.70±0.09
2088.1	134.56	14.67±0.19	820.5	150.72	13.66±0.08
1947.4	136.59	14.51±0.23	711.2	151.94	13.62±0.08
1806.1	138.55	14.35±0.19	615.4	152.98	13.58±0.07
1668.7	140.40	14.21±0.15	531.6	153.89	13.57±0.07
1537.3	142.11	14.13±0.14	436.4	154.91	13.54±0.07
1412.6	143.70	14.00±0.11	340.2	155.92	13.54±0.07
1295.4	145.15	13.93±0.10	251.6	156.85	13.50±0.07
1185.8	146.48	13.84±0.12	159.7	157.79	13.46±0.06
1083.7	147.69	13.78±0.11	108.1	158.29	13.46±0.06
		$T = 250$ K			
3248.1	140.74	17.11±0.16	1574.1	154.72	15.38±0.08
3122.6	141.77	16.93±0.15	1499.5	155.33	15.34±0.10
3029.8	142.56	16.76±0.13	1427.9	155.90	15.29±0.08
2927.7	143.42	16.65±0.13	1292.9	156.97	15.24±0.08
2820.3	144.33	16.52±0.17	1169.4	157.95	15.15±0.07
2711.1	145.25	16.39±0.14	1057.0	158.84	15.09±0.08
2602.0	146.18	16.25±0.11	954.4	159.65	15.05±0.07
2494.3	147.09	16.16±0.14	755.5	161.19	14.97±0.07
2388.8	147.98	16.05±0.12	667.7	161.87	14.94±0.07
2286.3	148.84	15.96±0.10	596.4	162.42	14.91±0.06
2186.1	149.68	15.88±0.11	507.1	163.10	14.89±0.07
2089.2	150.49	15.78±0.10	431.9	163.67	14.88±0.07
1995.3	151.27	15.71±0.10	353.9	164.27	14.86±0.06
1904.4	152.02	15.64±0.11	265.0	164.94	14.85±0.07
1817.4	152.73	15.56±0.10	183.3	165.56	14.79±0.07
1733.0	153.43	15.53±0.10	112.8	166.09	14.77±0.07
1652.2	154.09	15.43±0.08	106.8	166.14	14.76±0.08
1574.1	154.72	15.38±0.08			

Table VII. *(Continued)*

p (kPa)	c ($m \cdot s^{-1}$)	η ($\mu Pa \cdot s$)	p (kPa)	c ($m \cdot s^{-1}$)	η ($\mu Pa \cdot s$)
		$T = 275$ K			
3144.3	157.16	17.84±0.12	669.2	170.41	16.24±0.07
2907.1	158.29	17.59±0.11	557.7	171.03	16.20±0.06
2684.4	159.44	17.41±0.09	464.2	171.55	16.19±0.06
2475.2	160.54	17.24±0.10	352.4	172.18	16.17±0.06
2280.4	161.57	17.09±0.11	243.9	172.79	16.14±0.07
2098.8	162.55	16.96±0.08	140.6	173.36	16.08±0.07
1929.7	163.46	16.86±0.08	106.5	173.56	16.08±0.08
1772.8	164.32	16.75±0.09	667.7	161.87	14.94±0.07
1627.3	165.11	16.68±0.08	596.4	162.42	14.91±0.06
1492.6	165.85	16.59±0.08	507.1	163.10	14.89±0.07
1368.1	166.54	16.54±0.07	431.9	163.67	14.88±0.07
1253.2	167.17	16.47±0.07	353.9	164.27	14.86±0.06
1147.3	167.76	16.43±0.07	265.0	164.94	14.85±0.07
1049.8	168.30	16.39±0.07	183.3	165.56	14.79±0.07
960.1	168.80	16.34±0.07	112.8	166.09	14.77±0.07
802.2	169.67	16.29±0.07	106.8	166.14	14.76±0.08
		$T = 300$ K			
3145.5	169.23	18.82±0.10	1370.6	175.54	17.77±0.07
2961.5	169.79	18.70±0.09	1218.9	176.13	17.70±0.07
2833.8	170.22	18.60±0.09	1083.5	176.66	17.65±0.07
2698.5	170.67	18.52±0.09	962.5	177.14	17.61±0.07
2561.9	171.14	18.43±0.08	805.4	177.77	17.54±0.07
2427.7	171.61	18.34±0.09	673.4	178.30	17.51±0.07
2297.5	172.07	18.26±0.08	542.9	178.83	17.47±0.07
2172.2	172.52	18.19±0.08	406.1	179.39	17.45±0.06
1939.2	173.38	18.05±0.08	283.2	179.90	17.40±0.07
1728.9	174.16	17.94±0.07	197.2	180.26	17.34±0.07
1540.0	174.88	17.85±0.07	144.8	180.47	17.30±0.07
1370.6	175.54	17.77±0.07			
		$T = 325$ K			
3359.5	179.06	20.04±0.08	1660.9	182.99	19.10±0.06
3144.3	179.49	19.89±0.07	1469.3	183.50	19.01±0.06
2996.6	179.80	19.80±0.07	1299.0	183.96	18.94±0.06
2841.5	180.13	19.70±0.07	1148.1	184.38	18.88±0.06
2686.6	180.47	19.62±0.07	1014.1	184.75	18.84±0.06
2535.7	180.82	19.53±0.07	841.3	185.25	18.78±0.06
2390.6	181.16	19.46±0.07	649.3	185.80	18.71±0.07
2251.8	181.49	19.38±0.06	522.2	186.18	18.69±0.07
2120.1	181.81	19.31±0.06	382.7	186.60	18.65±0.08
1877.5	182.44	19.19±0.06	246.6	187.01	18.60±0.08

Table VII. *(Continued)*

p (kPa)	c ($m \cdot s^{-1}$)	η ($\mu Pa \cdot s$)	p (kPa)	c ($m \cdot s^{-1}$)	η ($\mu Pa \cdot s$)
		$T = 350$ K			
3243.5	188.49	21.01±0.15	1440.1	191.28	20.16±0.12
3055.2	188.73	20.91±0.15	1265.8	191.60	20.10±0.11
2952.9	188.86	20.85±0.15	1112.8	191.89	20.04±0.10
2822.1	189.04	20.79±0.15	977.8	192.16	20.00±0.10
2678.6	189.24	20.71±0.14	858.9	192.40	19.96±0.10
2532.0	189.45	20.64±0.14	754.0	192.61	19.92±0.10
2385.1	189.67	20.56±0.14	662.2	192.80	19.90±0.09
2244.8	189.89	20.51±0.13	544.6	193.05	19.87±0.09
2109.7	190.11	20.44±0.13	447.9	193.26	19.86±0.09
1981.3	190.32	20.38±0.12	345.1	193.48	19.84±0.08
1860.0	190.53	20.33±0.12	249.2	193.69	19.80±0.08
1745.2	190.73	20.29±0.12	148.5	193.91	19.77±0.09
1637.0	190.92	20.24±0.12	114.8	193.99	19.74±0.10
1535.6	191.10	20.20±0.12	107.4	194.02	19.75±0.09
		$T = 375$ K			
3088.1	197.00	21.98±0.13	1250.6	198.76	21.23±0.10
2867.2	197.14	21.87±0.12	1094.0	198.96	21.17±0.11
2719.3	197.25	21.80±0.11	956.7	199.14	21.13±0.07
2565.7	197.38	21.74±0.13	836.4	199.30	21.09±0.08
2413.4	197.51	21.66±0.11	731.2	199.45	21.07±0.10
2265.8	197.65	21.60±0.11	639.1	199.58	21.04±0.07
2124.7	197.79	21.55±0.11	522.1	199.74	21.02±0.07
1990.8	197.92	21.49±0.08	426.6	199.89	21.00±0.07
1864.0	198.06	21.45±0.12	326.0	200.04	20.99±0.08
1745.1	198.19	21.40±0.11	233.1	200.18	20.95±0.13
1633.1	198.31	21.36±0.11	137.0	200.33	20.92±0.14
1528.0	198.43	21.32±0.10	112.2	200.38	20.93±0.16
1429.4	198.55	21.29±0.10	104.7	200.40	20.93±0.18

[a] ρ calculated from Ref. 1.

the highest density (2746 $mol \cdot m^{-3}$ at 225 K and 2983 kPa), the present value for the speed of sound is 0.7% lower than the extrapolation. We believe the present data are more accurate than the extrapolation.

6.7. Hexafluoroethane

The viscosity of hexafluoroethane was measured along eight isotherms between 225 and 375 K, at pressures up to 3.3 MPa. Table VIII lists the

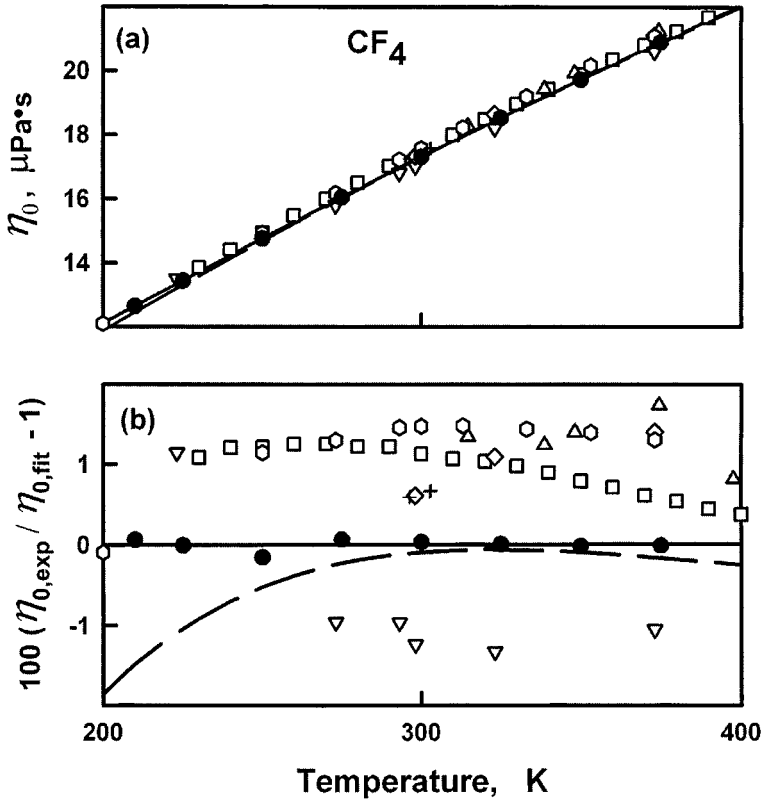

Fig. 6. (a) Zero-density viscosities of CF_4: (●), Present work; (—), Eq. (12); (□), Ref. 36; (△), Ref. 37; (▽), Ref. 38; (◇), Ref. 39; (○), Ref. 40; (+), Ref. 41; (---), Ref. 43. (b) Fractional deviations from Eq. (12) of data from the upper figure.

results. The equation of state of Hurly [1] was used to calculate density and C_p from the measured temperature and pressure, both to 0.1%. Thermal conductivities were taken from Thodos and Roy [42] who claim an uncertainty of 2%, with the density dependence taken from Ref 32. Each isotherm was fit by Eq. (10), and the results are listed in Table I. To display deviations, we represented our seven values of η_0 for C_2F_6 by the polynomial,

$$\eta_0(T)/\mu\text{Pa}\cdot\text{s} = -0.483 + 5.565\times10^{-2}\,(T/\text{K}) - (2.404\times10^{-5})\,(T/\text{K})^2 \quad (225\ \text{K} \leqslant T \leqslant 375\ \text{K}) \tag{13}$$

Table VIII. Viscosity (η) and Speed-of-Sound (c) Measurements in C_2F_6[a]

p (kPa)	c ($m \cdot s^{-1}$)	η ($\mu Pa \cdot s$)	p (kPa)	c ($m \cdot s^{-1}$)	η ($\mu Pa \cdot s$)
		$T = 225$ K			
352.3	112.01	10.84±0.05	221.7	116.17	10.84±0.04
330.8	112.75	10.83±0.05	201.7	116.77	10.84±0.04
318.1	113.16	10.84±0.04	183.4	117.31	10.85±0.04
305.1	113.56	10.83±0.04	166.6	117.80	10.84±0.04
292.1	113.97	10.83±0.04	131.0	118.82	10.83±0.04
279.4	114.38	10.82±0.04	113.2	119.32	10.84±0.04
267.0	114.77	10.84±0.04	93.3	119.87	10.82±0.05
255.0	115.15	10.82±0.04	80.6	120.22	10.83±0.06
		$T = 250$ K			
810.2	109.00	12.11±0.06	370.1	120.72	11.94±0.04
745.0	111.05	12.12±0.08	302.2	122.26	11.97±0.05
669.0	113.20	12.03±0.04	246.2	123.49	11.94±0.04
605.2	114.92	11.99±0.05	180.6	124.89	11.94±0.04
548.9	116.39	11.99±0.05	119.0	126.16	11.90±0.06
498.0	117.67	11.97±0.04	112.7	126.30	11.93±0.05
429.7	119.33	11.97±0.05	106.8	126.42	11.92±0.04
		$T = 275$ K			
1802.1	95.63	14.40±0.14	934.3	118.32	13.32±0.06
1769.3	96.79	14.29±0.11	846.5	120.07	13.29±0.06
1731.9	98.07	14.26±0.09	765.5	121.63	13.19±0.06
1685.6	99.57	14.26±0.10	691.1	123.02	13.16±0.05
1634.2	101.18	14.13±0.11	623.0	124.26	13.13±0.05
1579.4	102.82	14.08±0.14	560.8	125.37	13.11±0.04
1522.7	104.45	14.01±0.10	504.3	126.35	13.11±0.04
1464.9	106.04	13.86±0.08	429.2	127.63	13.07±0.05
1349.7	109.02	13.63±0.13	364.7	128.71	13.08±0.05
1293.1	110.41	13.66±0.08	292.9	129.89	13.05±0.05
1237.5	111.74	13.51±0.09	222.1	131.02	13.04±0.05
1183.2	112.99	13.54±0.06	150.4	132.15	13.03±0.06
1130.3	114.18	13.43±0.05	113.9	132.72	13.02±0.06
1028.8	116.37	13.37±0.06	107.5	132.82	13.03±0.06
		$T = 300$ K			
2565.5	100.57	16.92±0.16	1228.2	124.09	14.62±0.07
2472.4	102.53	16.61±0.12	1183.2	125.00	14.56±0.07
2404.5	103.91	16.43±0.13	1105.7	125.87	14.52±0.07
2328.3	105.44	16.25±0.19	1048.3	126.68	14.44±0.05
2246.7	107.03	16.14±0.18	993.5	127.46	14.45±0.05
2161.9	108.64	15.84±0.15	941.1	128.18	14.41±0.06
2075.9	110.24	15.73±0.18	843.2	129.52	14.30±0.06
1989.8	111.80	15.61±0.12	754.7	130.70	14.30±0.14
1904.5	113.30	15.41±0.09	674.8	131.76	14.22±0.14
1820.5	114.74	15.27±0.07	602.7	132.70	14.23±0.05
1738.3	116.12	15.15±0.07	537.8	133.54	14.20±0.04
1658.1	117.44	15.08±0.10	479.5	134.28	14.18±0.04
1580.1	118.70	14.98±0.09	403.4	135.24	14.17±0.04
1504.5	119.90	14.88±0.05	358.9	135.79	14.15±0.04
1431.6	121.03	14.79±0.07	291.7	136.62	14.14±0.04
1361.2	122.11	14.74±0.07	231.7	137.35	14.13±0.04
1293.4	123.13	14.69±0.08			

Table VIII. *(Continued)*

p (kPa)	c ($m \cdot s^{-1}$)	η ($\mu Pa \cdot s$)	p (kPa)	c ($m \cdot s^{-1}$)	η ($\mu Pa \cdot s$)
		$T = 325$ K			
2939.1	114.82	18.04 ± 0.09	1448.8	131.28	15.86 ± 0.04
2815.7	116.19	17.74 ± 0.11	1370.4	132.10	15.75 ± 0.05
2725.0	117.22	17.48 ± 0.11	1295.6	132.88	15.69 ± 0.04
2625.3	118.35	17.41 ± 0.08	1156.3	134.31	15.59 ± 0.04
2520.1	119.54	17.15 ± 0.09	1030.5	135.59	15.49 ± 0.04
2413.0	120.75	16.95 ± 0.07	917.2	136.73	15.43 ± 0.04
2305.3	121.96	16.78 ± 0.07	815.3	137.75	15.37 ± 0.04
2198.8	123.15	16.66 ± 0.06	723.9	138.65	15.35 ± 0.04
2094.3	124.31	16.50 ± 0.06	642.2	139.45	15.29 ± 0.05
1992.4	125.44	16.39 ± 0.06	569.2	140.16	15.26 ± 0.04
1893.3	126.52	16.27 ± 0.06	474.5	141.07	15.23 ± 0.04
1797.4	127.56	16.16 ± 0.06	395.1	141.83	15.21 ± 0.05
1705.0	128.56	16.06 ± 0.06	309.3	142.65	15.18 ± 0.05
1616.0	129.51	15.93 ± 0.05	229.6	143.40	15.17 ± 0.06
1530.5	130.42	15.98 ± 0.04	142.7	144.21	15.13 ± 0.06
		$T = 350$ K			
3132.6	127.56	18.74 ± 0.11	1483.1	139.72	16.82 ± 0.06
2995.9	128.48	18.54 ± 0.11	1317.7	140.97	16.70 ± 0.04
2894.9	129.18	18.33 ± 0.08	1168.7	142.09	16.61 ± 0.05
2668.0	130.82	18.05 ± 0.07	1035.0	143.10	16.51 ± 0.05
2549.0	131.69	17.92 ± 0.07	915.4	144.00	16.45 ± 0.04
2428.9	132.58	17.75 ± 0.06	808.7	144.80	16.39 ± 0.05
2310.4	133.47	17.63 ± 0.07	713.7	145.51	16.34 ± 0.04
2194.1	134.34	17.49 ± 0.07	629.4	146.14	16.31 ± 0.04
2080.8	135.19	17.36 ± 0.05	520.5	146.95	16.28 ± 0.04
1971.1	136.02	17.26 ± 0.05	430.1	147.62	16.24 ± 0.04
1865.1	136.82	17.17 ± 0.05	333.2	148.33	16.21 ± 0.04
1763.3	137.59	17.05 ± 0.06	270.0	148.80	16.20 ± 0.04
1665.7	138.33	16.97 ± 0.05	194.5	149.36	16.17 ± 0.05
1572.3	139.04	16.90 ± 0.05	147.9	149.70	16.15 ± 0.05
1483.1	139.72	16.82 ± 0.06	97.0	150.08	16.14 ± 0.06
		$T = 375$ K			
3180.6	138.51	19.45 ± 0.10	1429.3	147.65	17.73 ± 0.05
3015.9	139.29	19.27 ± 0.07	1343.2	148.13	17.69 ± 0.05
2906.1	139.83	19.13 ± 0.06	1184.8	149.03	17.58 ± 0.06
2785.4	140.41	18.99 ± 0.06	1043.5	149.83	17.49 ± 0.05
2660.8	141.03	18.84 ± 0.06	917.9	150.55	17.43 ± 0.05
2534.6	141.67	18.69 ± 0.05	806.5	151.18	17.37 ± 0.04
2408.1	142.33	18.56 ± 0.05	708.1	151.75	17.34 ± 0.04
2283.9	142.98	18.44 ± 0.05	621.2	152.25	17.27 ± 0.04
2162.2	143.62	18.33 ± 0.06	510.1	152.89	17.24 ± 0.06
2044.1	144.26	18.22 ± 0.05	418.4	153.42	17.20 ± 0.05
1930.2	144.88	18.13 ± 0.05	319.2	153.99	17.17 ± 0.05
1820.6	145.48	18.03 ± 0.05	240.8	154.44	17.13 ± 0.05
1715.5	146.05	17.96 ± 0.05	148.1	154.98	17.12 ± 0.06
1615.4	146.61	17.88 ± 0.06	117.4	155.16	17.10 ± 0.07
1520.0	147.14	17.80 ± 0.05	86.8	155.33	16.65 ± 0.11

[a] ρ calculated from Ref. 1.

with a fractional standard deviation of 0.0016. Figure 7a shows the measured viscosity as a function of temperature, and Fig 7b shows the relative deviations from Eq. (13). Also shown are the previously published measurements of the viscosity of C_2F_6 [38, 43–45]. The scatter in the previously published values is about 5%, the present values are accurate to within 0.5%, greatly reducing the uncertainty in the viscosity of this fluid.

Figure 5b compares the present speed-of-sound data at 300 K with those in Ref. 1 in the range of overlap (up to 700 mol·m^{-3}). They disagree by 0.07% to 0.15%, and similar disagreements occur on the other isotherms. This disagreement was traced to the presence of a volatile

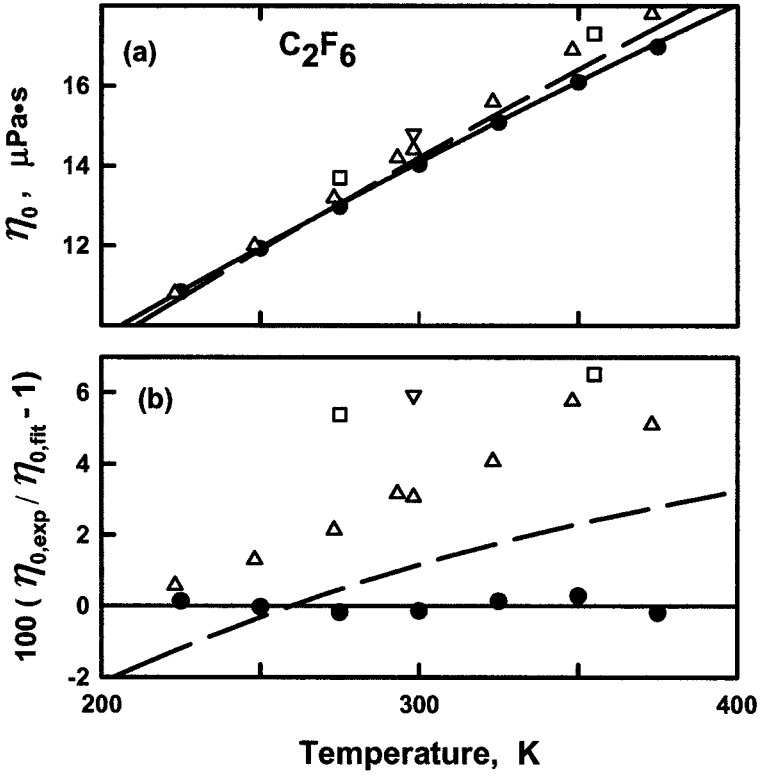

Fig. 7. (a) Zero-density viscosities in C_2F_6: (●), Present work; (—), Eq. (13); (△), Ref. 38; (▽), Ref. 44; (□), Ref. 45; (---), Ref. 43. (b) Fractional deviations from Eq. (13) of the data in the upper figure.

impurity with a concentration exceeding that specified by the manufacturer. Thus, the speed-of-sound results from Ref. 1 are more reliable than the present results in the range of overlap. At densities well above the range of overlap, the present speed-of-sound results are probably more accurate than the extrapolation from Ref. 1. We believe that the impurity had a negligible effect on the viscosity results.

7. DISCUSSION

We calibrated the Greenspan viscometer with helium and then we assessed its performance with argon and four polyatomic gases. The argon results spanned the range 293 K $< T <$ 375 K and 0.15 MPa $< p <$ 3.3 MPa. They agreed (to within 0.3% at zero density; to within 0.5% up to 1500 mol $\cdot$ m^{-3}) with independent measurements made using different techniques: oscillating disks [22], vibrating wires [14], and rotating cylinders [17]. The results from the polyatomic gases CH_4, C_3H_8, N_2, and SF_6 near 300 K show that the viscometer and its model properly account for the diverse thermophysical properties of these gases. Typically, the present results for the polyatomic gases agreed with reference values to within 0.5%. At the higher densities (particularly for SF_6), it is conceivable that the uncertainty of the reference viscosities exceeds 0.5%.

Additional measurements were made in the gases CF_4 and C_2F_6 spanning the temperature range 210 to 375 K and pressures up to 3.3 MPa. Previously, only zero-density viscosities were reported for these compounds and they had reported uncertainties of several percent. The uncertainty of the present results for these gases is approximately 0.5% at low densities, as indicated by the results with the reference gases. This estimate would be true even if the reported thermal conductivities of CF_4 and C_2F_6 were in error by several times the uncertainty ($\Delta\lambda/\lambda = 0.02$) attributed to them by Refs. 35 and 42.

We plan to measure the viscosity of several gases for which no previous measurements of viscosity or thermal conductivity have been published. In these cases, the thermal conductivity must be estimated and might have uncertainties of 10 to 20%. Fortunately, the factor $(\gamma - 1)$ that appears in Eq. (6) is small for many of these compounds at the low densities where they are used.

ACKNOWLEDGMENT

This research was supported in part by NIST's Office of Microelectronics Programs.

REFERENCES

1. J. J. Hurly, *Int. J. Thermophys.* **20**:455 (1999).
2. M. Greenspan and F. N. Wimenitz, *An Acoustic Viscometer for Gases-I*, NBS Report 2658 (1953).
3. K. A. Gillis, J. B. Mehl, and M. R. Moldover, *Rev. Sci. Instrum.* **67**:1850 (1996).
4. K. A. Gillis, J. B. Mehl, and M. R. Moldover, *J. Acous. Soc. Amer.* **114**:166 (2003).
5. J. Wilhelm, K. A. Gillis, J. B. Mehl, and M. R. Moldover, *Int. J. Thermophys.* **21**:983 (2000).
6. J. J. Hurly and M. R. Moldover, *J. Res. Natl. Inst. Stand. Technol.* **105**:667 (2000).
7. J. Kestin, R. Paul, A. A. Clifford, and W. A. Wakeham, *Physica A* **100**:349 (1980).
8. J. R. Olson and G. W. Swift, *J. Acoust. Soc. Am.* **100**:2123 (1996).
9. J. B. Mehl, *J. Acoust. Soc. Am.* **97**:3327 (1995).
10. J. B. Mehl, *J. Acoust. Soc. Am.* **106**:73 (1999).
11. J. Kestin and W. Leidenfrost, *Physica* **25**:1033 (1959).
12. J. J. Hurly, J. W. Schmidt, S. J. Boyes, and M. R. Moldover, *Int. J. Thermophys.* **18**:579 (1997).
13. J. B. Mehl and M. R. Moldover, *J. Chem. Phys.* **77**:455 (1982).
14. J. Wilhelm and E. Vogel, *Int. J. Thermophys.* **21**:301 (2000).
15. A. F. Estrada-Alexanders and J. P. M. Trusler, *Int. J. Thermophys.* **17**:1325 (1996).
16. L. Sun, J. E. S. Venart, and R. C. Prasad, *Int. J. Thermophys.* **23**:357 (2002).
17. C. Evers, H. W. Lösch, and W. Wagner, *Int. J. Thermophys.* **23**:1411 (2002).
18. E. Vogel, *Ber. Bunsenges. Phys. Chem.* **88**, 997 (1984).
19. E. Bich, J. Millat, and E. Vogel, *J. Phys. Chem. Ref. Data* **6**:1289 (1990).
20. J. P. M. Trusler and M. Zarari, *J. Chem. Thermodyn.* **24**:973 (1992).
21. B. A. Younglove and J. F. Ely, *J. Phys. Chem. Ref. Data* **16**:577 (1987).
22. E. Vogel, J. Wilhelm, C. Küchenmeister, and M. Jaeschke, *High Temp.-High Press.* **32**:73 (2000).
23. R. Span and W. Wagner, private communication.
24. K. N. Marsh, R. A. Perkins, and M. L. V. Ramires, *J. Chem. Eng. Data* **47**:932 (2002).
25. R. Span, E. W. Lemmon, R. T Jacobsen, W. Wagner, and A. Yokozeki, *J. Phys. Chem. Ref. Data* **29**:1361 (2000).
26. R. A. Perkins, H. M. Roder, D. G. Friend, and C. A. Nieto de Castro, *Physica A* **173**:332 (1991).
27. J. F. Estela-Uribe and J. P. M. Trusler, *Int. J. Thermophys.* **21**:1033 (2000).
28. A. J. Zuckerwar and W. A. Griffin, *J. Acoust. Soc. Am.* **69**:150 (1981).
29. J. Kestin, E. Paykosc, and J. V. Sengers, *Physica* **54**:1 (1971).
30. J. J. Hurly, D. R. Defibaugh, and M. R. Moldover, *Int. J. Thermophys.* **21**:739 (2000).
31. E. P. Zherdev, S. A. Olbybin, and S. S. Bakalin, *Teplofiz. Vys. Temp.* **14**:391 (1976).
32. M. O. McLinden, S. A. Klein, and R. A. Perkins, *Int. J. Refrig.* **23**:43 (2000).
33. D. L. Timrot, M. A. Serednitskaya, and S. A. Traktueva, *Teplofiz. Vys. Temp.* **13**:1112 (1975).
34. T. Strehlow and E. Vogel, *Physica A* **161**:101 (1989).
35. F. J. Uribe, K. A. Mason, and J. Kestin, *J. Phys. Chem. Ref. Data* **19**:1123 (1990).
36. *Thermophysical Properties of Matter* (IFI/Plenum, New York, 1970).
37. J. Timmermans, *Physico-Chemical Constants of Pure Organic Substances*, 2nd Ed. (Elsevier, New York, 1965).
38. Matheson Gas Data Book, unabridged Ed. (Matheson Company, East Rutherford, New Jersey, 1974).
39. J. M. Hellemans, *Physica* **65**:376 (1973).

40. E. A. Mason, J. Kestin, J. Bzowski, and A. Bousheri, *J. Phys. Chem. Ref. Data* **16**:445 (1987).
41. W. A. Wakeham, S. T. Ro, and J. Kestin, *Trans. Farad. Soc.* **67**:2308 (1971).
42. G. Thodos and D. Roy, *Ind. Eng. Chem. Fundam.* **7**:529 (1968).
43. S. A. Klein, M. O. McLinden, and A. Laesecke, *Int. J. Refrig.* **20**:208 (1997).
44. Freon Products, E. I. DuPont de Nemours and Co. (Freon Products Division, Wilmington, Delaware, 1969).
45. D. Reichenberg, *The Viscosity of Organic Vapors at Low Pressures*, DSC Rep. 11, (National Physical Laboratory, Teddington, England, August 1971).